JOURNAL OF NEUROTRAUMA 29:813–827 (March 20, 2012)

DOI: 10.1089/neu.2011.1980

Cyclin D1 Gene Ablation Confers Neuroprotection in Traumatic Brain Injury

Shruti V. Kabadi,[1,2] Bogdan A. Stoica,[1,2] David J. Loane,[1,2] Kimberly R. Byrnes,[2,3] Marie Hanscom,[1] Rainier M. Cabatbat,[1,2] Ming T. Tan,[4] and Alan I. Faden[1,2]

Abstract

Cell cycle activation (CCA) is one of the principal secondary injury mechanisms following brain trauma, and it leads to neuronal cell death, microglial activation, and neurological dysfunction. Cyclin D1 (CD1) is a key modulator of CCA and is upregulated in neurons and microglia following traumatic brain injury (TBI). In this study we subjected CD1-wild-type ($CD1^{+/+}$) and knockout ($CD1^{-/-}$) mice to controlled cortical impact (CCI) injury to evaluate the role of CD1 in post-traumatic neurodegeneration and neuroinflammation. As early as 24 h post-injury, $CD1^{+/+}$ mice showed markers of CCA in the injured hemisphere, including increased CD1, E2F1, and proliferating cell nuclear antigen (PCNA), as well as increased Fluoro-Jade B staining, indicating neuronal degeneration. Progressive neuronal loss in the hippocampus was observed through 21 days post-injury in these mice, which correlated with a decline in cognitive function. Microglial activation in the injured hemisphere peaked at 7 days post-injury, with sustained increases at 21 days. In contrast, $CD1^{-/-}$ mice showed reduced CCA and neurodegeneration at 24 h, as well as improved cognitive function, attenuated hippocampal neuronal cell loss, decreased lesion volume, and cortical microglial activation at 21 days post-injury. These findings indicate that CD1-dependent CCA plays a significant role in the neuroinflammation, progressive neurodegeneration, and related neurological dysfunction resulting from TBI. Our results further substantiate the proposed role of CCA in post-traumatic secondary injury, and suggest that inhibition of CD1 may be a key therapeutic target for TBI.

Key words: cell cycle; controlled cortical impact; cyclin D1; neuroinflammation; neuroprotection

Introduction

Traumatic brain injury (TBI) represents a major public health problem, with more than 1.7 million new cases annually in the United States (Faul et al., 2010), accounting for 60% of all emergency department admissions and 50% of all trauma deaths (Dutton et al., 2010). TBI causes cell death and neurological dysfunction through both direct physical disruption of tissue (primary injury), as well as through delayed and potentially reversible molecular and cellular pathophysiological mechanisms that cause progressive white and grey matter damage (secondary injury; Loane and Faden, 2010). Such delayed injury begins within seconds to minutes after the insult, and may continue for days, weeks, or potentially months to years (Bramlett and Dietrich, 2007), and may be responsible for a significant component of the neurodegeneration and neurological impairment seen following TBI (Loane and Faden, 2010). Some of the more important secondary injury mechanisms involve intrinsic neuronal cell death pathways, microglial activation, and secondary neurotoxicity.

Previous studies have linked cell cycle events and neuronal cell death. Historically, post-mitotic cells such as neurons were thought to have permanently entered G0 phase and were incapable of entering the cell cycle. However, recent studies indicate that cell cycle re-entry of mature differentiated post-mitotic neurons occurs, but results in apoptosis rather than neuronal proliferation (Herrup and Yang, 2007; Kranenburg et al., 1996). The normal cell cycle is controlled by complex molecular mechanisms and progression through cell

[1]Center for Shock, Trauma and Anesthesiology Research (STAR), and the Department of Anesthesiology, University of Maryland, School of Medicine, Baltimore, Maryland.
[2]Department of Neuroscience, Georgetown University Medical Center, Washington, D.C.
[3]Department of Anatomy, Physiology and Genetics, Uniformed Services University, Bethesda, Maryland.
[4]Division of Biostatistics, University of Maryland, Greenebaum Cancer Center, Baltimore, Maryland.

cycle phases that require sequential activation of a large group of Ser/Thr kinases called the cyclin-dependent kinases (CDK) and their positive regulators (cyclins; Arendt, 2003). The first stage of the cell cycle, the G1 phase, is initiated sequentially by increased levels of members of the cyclin D family, activation of cyclin D-dependent kinase activity, phosphorylation of the retinoblastoma (Rb) family, and activation of the E2F (E2 promoter binding factor) family of transcription factors. Active E2F induces transcription of various genes involved in cell cycle, ultimately resulting in mitosis (Stoica et al., 2009).

In contrast, in post-mitotic neurons increased levels of cyclin D and phosphorylation of Rb are associated with programmed cell death (Freeman et al., 1994). This may reflect the fact that in neurons, active E2Fs can contribute to increased transcription of pro-apoptotic molecules such as caspases-3, -9, and -8, and Apaf-1 or Bcl-2 family members (Greene et al., 2004; Nguyen et al., 2003). Central nervous system (CNS) injuries such as TBI induce cell cycle activation (CCA) not only in neurons, but also in glial cells; this can result either in the apoptosis of post-mitotic glial cells (mature oligodendroglia), or in the proliferation and activation of glial cells such as astroglia and microglia. Microglial activation can be associated with the release of pro-inflammatory and neurotoxic molecules (Byrnes and Faden, 2007; Giovanni et al., 2005). Therefore, CCA following TBI may initiate multiple secondary injury mechanisms that include neuronal and oligodendroglial apoptosis, as well as more delayed effects such as microglial activation and potentially astroglial scar formation.

A potential target for blocking cell cycle pathways is cyclin D1 (CD1), an early regulator of cell cycle re-entry. Increased expression of CD1 has been observed in microglia and astrocytes within 24 h of TBI (Giovanni et al., 2005). In addition, there is increased localization of CD1 in cortical neurons following TBI, with many CD1 neurons being positive for activated caspase-3, supporting the connection between cell cycle activation and neuronal cell death (Cernak et al., 2005; Giovanni et al., 2005). To address this issue, we examined the effects of knockout of the CD1 gene on CCA and secondary injury after TBI. We present a comprehensive quantitative assessment of neuronal cell loss and microglial activation after TBI using a well-established murine model of controlled cortical impact (CCI). CD1 gene knockout (−/−) and wild-type (+/+) mice were compared to assess the role of CD1 and CCA in the progressive neurodegeneration, neuroinflammation, and associated chronic neurological dysfunction after TBI.

Methods

Controlled cortical impact injury

All surgical procedures were carried out in accordance with protocols approved by the Georgetown University Animal Care and Use Committee. Our custom-designed CCI injury device (Fox et al., 1998; Loane et al., 2009) consists of a microprocessor-controlled pneumatic impactor with a 3.5-mm-diameter tip. CD1-knockout mice ($CD1^{-/-}$) of the C57BL/6J strain have been previously described and have a genetic background of 129 (129S2-derived D3 ES cell line)/C57BL/6 (Fantl et al., 1995; Landis et al., 2006; Sherr and Roberts, 2004; Sicinski et al., 1995). For our study, the CD1 mouse colony was generated from heterozygous breeders, which were generously donated by Dr. Richard G. Pestell at Georgetown University. $CD1^{+/+}$ and $CD1^{-/-}$ mice (20–25 g) were anesthetized with isoflurane (induction at 4% and maintenance at 2%) evaporated in a gas mixture containing 70% N_2O and 30% O_2 and administered through a nose mask. Depth of anesthesia was assessed by monitoring respiratory rate and pedal withdrawal reflexes. The mouse was placed on a heated pad, and core body temperature was maintained at 37°C. The head was mounted in a stereotaxic frame, and the surgical site was clipped and cleaned with chlorhexidine diacetate and ethanol scrubs. A 10-mm midline incision was made over the skull, the skin and fascia were reflected, and a 4-mm craniotomy was made on the central aspect of the left parietal bone. The impounder tip of the injury device was then extended to its full stroke distance (44 mm), positioned on the surface of the exposed dura, and reset to impact the cortical surface. Moderate injury was induced using an impactor velocity of 6 m/sec and deformation depth of 2 mm, as previously described (Loane et al., 2009). After injury, the incision was closed with interrupted 6-0 silk sutures, anesthesia was terminated, and the animal was placed in a heated cage to maintain normal core temperature for 45 min post-injury. All animals were monitored carefully for at least 4 h after surgery and then daily. Sham animals underwent the same procedure as injured mice except for the impact.

Immunocytochemistry

At 24 h after injury, the mice ($n = 3$/group) were anesthetized and transcardially perfused with saline and 10% buffered formalin phosphate solution. The brains were removed, post-fixed in paraformaldehyde for 24 h, and protected in 30% sucrose. Frozen brain sections (60 μm and 20 μm) were cut on a cryostat and mounted on glass slides. Selected slides were with stained with Fluoro-Jade B (Chemicon, Temecula, CA) to identify degenerating neurons, following the manufacturer's protocol. For immunocytochemistry, the sections were stained as previously described (Hilton et al., 2008), using one or more antibodies recognizing the following markers of cell cycle activation: CD1 (ab10540; Abcam, Cambridge, MA), PCNA (ab18197; Abcam), and E2F1 (554213; BD Pharmingen, San Diego, CA). Imaging based on fluorescence microscopy was carried out using a Leica TCS SP5 II Tunable Spectral Confocal microscope (Leica Microsystems Inc., Bannockburn, IL). For the acquisition of immunofluorescence images we used the "Tile Scan" function of the Leica Application Suite Advanced Fluorescence software (Leica LAS AF version 2.4.1) to scan multiple partial images of the injured brain hemisphere. The Scan Field was selected to cover the entire hemisphere. The "Merge Images" command was activated to automatically join the partial images into a complete image after the scan. The acquisition parameters were the same across all specimens: XY format 1024×1024; image size 775 μm×775 μm; zoom 1; speed 600 Hz; Pinhole Airy 1; Bi-directional X; same gain; autofocus-best focus noise-based method; tile scan auto-stitching and smooth; sequential scan between frames. The higher-magnification images were cropped from the indicated locations in the merged image.

Western immunoblot

At 21 days post-injury, mice ($n = 4$/group) were anesthetized (100 mg/kg sodium pentobarbital IP), transcardially

perfused with ice-cold saline, and decapitated. A 5-mm area surrounding the lesion epicenter on the ipsilateral cortex was rapidly dissected and immediately frozen on dry ice. Cortical tissue was homogenized in RIPA buffer and centrifuged at 15,000 rpm for 15 mins at 4°C to isolate proteins, and protein concentration was determined using the Pierce BCA Protein Assay kit (Thermo Scientific, Rockford, IL). Then 25 μg of protein was run on SDS polyacrylamide gel electrophoresis and transferred onto nitrocellulose membranes. The blots were then probed with antibodies against CD1 (1:2000; Lab Vision Products, Fremont, CA), and Iba-1 (1:1000; Wako Chemicals, Richmond, VA). β-Actin (1:20,000; Sigma-Aldrich, St. Louis, MO) was used as an endogenous control. Immune complexes were detected with the appropriate HRP-conjugated secondary antibodies (Kirkegaard & Perry Laboratories, Inc., Gaithersburg, MD), and visualized using SuperSignal West Dura Extended Duration Substrate (Thermo Scientific). Chemiluminescence was captured on a Kodak Image Station 4000R station (Carestream Health Inc., Rochester, NY), and protein bands were quantified by densitometric analysis using Carestream Molecular Imaging Software (Carestream Health Inc.). The data presented reflect the intensity of target protein bands compared to controls, and normalized based on the intensity of the endogenous control for each sample (expressed in arbitrary units).

Functional assessment

Morris Water Maze. Spatial learning and memory was assessed using an acquisition paradigm of the Morris Water Maze (MWM) test on post-injury days 14, 15, 16, and 17, as described previously (Fox et al., 1998; Loane et al., 2009). A white circular pool was divided into four quadrants using the computer-based AnyMaze video tracking system (Stoelting Co., Wood Dale, IL) and the platform was hidden in one quadrant (southwest) 14 inches from the side wall. Spatial learning and memory performance was assessed by determining the latency (in seconds) to locate the submerged hidden platform with a 90-sec limit per trial. Reference spatial memory was assessed by a probe trial carried out on post-injury day 18, as the time spent (in seconds) with a 60-sec limit in the quadrant where the platform had been hidden during the acquisition phase ($n = 12$–16/group). A visual cue test was subsequently performed on post-injury day 18 using a flagged platform placed on the platform in one of the quadrants (with a 90-sec limit per trial), and latency (in seconds) to locate the flagged platform was recorded.

Novel object recognition. Retention or intact memory was assessed by the novel object recognition (NOR) test on post-injury day 21. The apparatus consists of an open field (22.5 × 22.5 cm) with two adjacently-located imaginary circular zones, as previously designed (Bevins and Besheer, 2006). The zones are equally spaced from the sides in the center of the square and designated as "old object" and "novel object" zones using the AnyMaze video tracking system. The old object used was square-shaped, whereas the novel object was L-shaped, assembled using building blocks from Lego toys, and were clearly distinct in shape and appearance. On post-injury day 20, all animals ($n = 12$–16/group) were placed in the open field for 5 min each without any objects present for habituation. Two trials, 5 min each, were performed: the first (training) trial with two old objects in both the zones, and the second (testing) phase with one old object and one novel object present in the respective zones of the open field. There was an inter-trial interval of 60 min, during which the animals were placed back in their cages. The cognitive outcomes were calculated as the "discrimination index" (D.I.) for the second trial using the following formula:

$$\%\ D.I. = \frac{\text{time spent in novel object zone}}{(\text{time spent in old object zone} + \textit{time spent in novel object zone})} \times 100$$

All functional studies were performed by an investigator blinded to the groups.

Magnetic resonance imaging analysis

T2-weighted magnetic resonance imaging (MRI) at 21 days was used to measure lesion volume following TBI on a randomized subset of animals ($n = 3$–4/group), as previously detailed (Faden et al., 2003; Loane et al., 2009). Briefly, anesthetized animals were placed in a heated acrylic glass holder and a respiratory motion detector was positioned over the thorax to facilitate respiratory gating. The acrylic glass holder was then placed in the center of the 7-Tesla magnet bore (Bruker Medical Inc., Billerica, MA), where a 72-mm proton-tuned birdcage coil was positioned. Field homogeneity across the brain was optimized and a sagittal scout image was acquired (rapid acquisition relaxation enhancement pulse sequence [RARE] image; field of vision = 4 × 4 cm, 128 × 128 resolution, repetition time [TR] to echo time [TE] = 1500:10 msec with a RARE factor of 8, making the effective TE 40 msec). Multi-slice, multi-echo T2-weighted images were acquired using the following parameters: 3 × 3 cm FOV, 256 × 256 resolution, 1500:10 msec TR:TE, 8 RARE factor, TE = 40 msec, 10 slices, 0.75 mm slice thickness. Lesion volume was quantified from the summation of areas of hyperintensity on each slice, multiplied by slice thickness, for both the ipsilateral and contralateral hemispheres. Contralateral volumes were subtracted from ipsilateral volumes to obtain TBI-induced lesion volumes.

Histology

Mice were anesthetized and transcardially perfused with saline and 10% buffered formalin phosphate solution (containing 4% paraformaldehyde; Fisher Scientific, Pittsburgh, PA) at 24 h, 7 days, or 21 days after injury. The brains were removed, post-fixed in paraformaldehyde for 24 h, and protected in 30% sucrose. Frozen brain sections (60 μm and 20 μm) were cut on a cryostat and mounted onto glass slides. Every fourth 60-μm section was processed for immunohistochemical analysis beginning from a random start point. Microglia were immunostained with anti-Iba-1 (1:1000; Wako Chemicals) overnight, washed in PBS, and incubated with biotinylated anti-rabbit IgG antibody (Vector Laboratories, Burlingame, CA) for 2 h at room temperature. The sections were placed in avidin-biotin-horseradish peroxidase solution, diluted according to the manufacturer's instructions for 1 h (Vectastain Elite ABC kit; Vector Laboratories), and then reacted with 3,3′-diaminobenzidine (Vector Laboratories) for color development. Sections were counter-stained with cresyl violet (FD NeuroTechnologies, Baltimore, MD), dehydrated, and mounted for analysis.

Estimation of lesion volume ($n=5$–6/group). Lesion volume was estimated based on the Cavalieri method of unbiased stereology using Stereologer 2000 software (Systems Planning and Analysis, Alexandria, VA). Volumes of the ipsilateral and contralateral hemispheres were determined using the Cavalieri estimator with a grid spacing of 1 mm. Out of the total of 96 60-μm sections, every fourth section was analyzed beginning from a random start point. Lesion volume was estimated by subtracting the volume of the ipsilateral hemisphere from that of the contralateral hemisphere.

Assessment of neuronal cell loss in hippocampal sub-regions ($n=3$–4/group). StereoInvestigator software (MBF Biosciences, Williston, VT) was used to count the total number of surviving neurons in the cornu ammonis (CA)1, CA2/3, and the dentate gyrus (DG) sub-regions of the hippocampus using the optical fractionator method of unbiased stereology. Every fourth 60-μm section between -1.22 mm and -2.54 mm from the bregma was analyzed beginning from a random start point. The optical dissector had a size of 50 μm by 50 μm in the x- and y-axis, respectively, with a height of 10 μm and guard zone of 4 μm from the top of the section. The sampled region for each hippocampal subfield was demarcated in the injured hemisphere, and cresyl violet neuronal cell bodies were counted. For the CA1 and CA2/3 sub-regions, a grid spacing of 75 μm in the x-axis and 100 μm in the y-axis was used, resulting in an area fraction of one-twelfth. For the DG sub-region, a grid spacing of 175 μm in the x-axis and 100 μm in the y-axis was used, resulting in an area fraction of one twenty-eighth. The volume of the hippocampal subfield was measured using the Cavalieri estimator method with a grid spacing of 50 μm. The estimated number of surviving neurons in each field was divided by the volume of the region of interest to obtain the cellular density expressed in counts/mm^3.

Assessment of microglial morphology in the cortex ($n=3$–4/group). StereoInvestigator software was used to count the number of cortical microglia of each of the three microglial morphological phenotypes (ramified, hypertrophic, and bushy) using the optical fractionator method of unbiased stereology. The sampled region was the ipsilateral cortex between -1.22 mm and -2.54 mm from the bregma. Every fourth 60-μm section was analyzed beginning from a random start point. The sections were analyzed using a Leica DM4000B microscope (Leica Miocrosystems Inc.). The optical dissector had a size of 50 μm by 50 μm in the x- and y-axis, respectively, with a height of 10 μm and guard zone of 4 μm from the top of the section. For the cortex, a grid spacing of 150 μm in the x-axis and 150 μm in the y-axis was used, resulting in an area fraction of one-ninth. Microglial phenotypic classification was based on the length and thickness of the projections, the number of branches, and the size of the cell body, as previously described (Soltys et al., 2001). The volume of the region of interest was measured using the Cavalieri estimator method, with a grid spacing of 100 μm for the cortex. The estimated number of microglia in each phenotypic class was divided by the volume of the region of interest to obtain the cellular density expressed in counts/mm^3.

Neurolucida software (MBF Biosciences) was used to create reconstructions of microglia at different stages of activation following injury by tracing the cell bodies and processes. Microglia were outlined using the live image setting so that the width of the processes could be traced while focusing on the section accurately. The cell bodies were outlined using the contour tool, followed by tracing of the individual processes, using the dendrite line tool.

Statistical analysis

Lesion volume, functional data, and unbiased stereological analyses were performed by an investigator blinded to group. Quantitative data were expressed as mean ± standard error of the mean (SEM). Lesion volume was analyzed by one-tailed paired Student's *t*-test. Functional data (latency to find the platform) for the acquisition phase of the MWM were analyzed by repeated-measures (trial/time) two-way (genotype and injury/sham) analysis of variance (ANOVA), followed by *post-hoc* adjustments using Tukey's test to determine the interactions of post-injury days, injury/sham, and genotype. The two genotypes ($CD1^{+/+}$ and $CD1^{-/-}$) in the sham and injured groups were separately analyzed by repeated-measures (trial/time) one-way (genotype) ANOVA, followed by *post-hoc* adjustments using Tukey's test. The cognitive function data in the probe trial of the MWM (time spent in target quadrant), and the NOR (discrimination index) test were analyzed by two-way (group and injury/sham) ANOVA, followed by *post-hoc* adjustments using Tukey's test. The two genotypes ($CD1^{+/+}$ and $CD1^{-/-}$) in the sham and injured groups were separately analyzed by one-tailed paired Student's *t*-test. The analysis of time-course-based stereological data was performed by one-way ANOVA, followed by *post-hoc* adjustments using Tukey's test for comparisons across different time points. In addition, a one-tailed paired Student's *t*-test was performed versus the $CD1^{+/+}$ group at each time point. Regression analysis between cognitive improvement and stereological assessment (DG neuronal cell loss), and lesion volume by histology and MRI, was performed by linear regression and a correlation coefficient (r^2) was determined. The data for expression of biochemical markers using Western blotting were analyzed by a one-tailed paired Student's *t*-test, versus the sham and $CD1^{+/+}$ groups. The functional data were analyzed using SigmaStat, Version 3.5 (Systat Software, San Jose, CA). All other statistical tests were performed using GraphPad Prism software, version 3.02 for Windows (GraphPad Software, San Diego, CA).

Results

$CD1^{-/-}$ mice have reduced cell cycle activation and degenerating neurons after TBI

To determine the effects of CD1 knockout on TBI-induced neurodegeneration, we performed Fluoro-Jade B staining at 24 h after TBI. Representative confocal merged (Fig. 1–1) and higher-magnification images (Fig. 1–1a–f) from the injured hemisphere in $CD1^{+/+}$ mice demonstrate a large number of degenerating (Fluoro-Jade B-positive) neurons, located around the lesion site (Fig. 1–1a, b, and f), and in sub-cortical areas (Fig. 1–1c–e). In contrast, injured $CD1^{-/-}$ mice had less intense Fluoro-Jade B staining overall (Fig. 1–2a–f), including regions around the injury site in the cortex (Fig. 1–2a and f), and sub-cortical areas (Fig. 1–2b–e), suggesting fewer degenerating neurons.

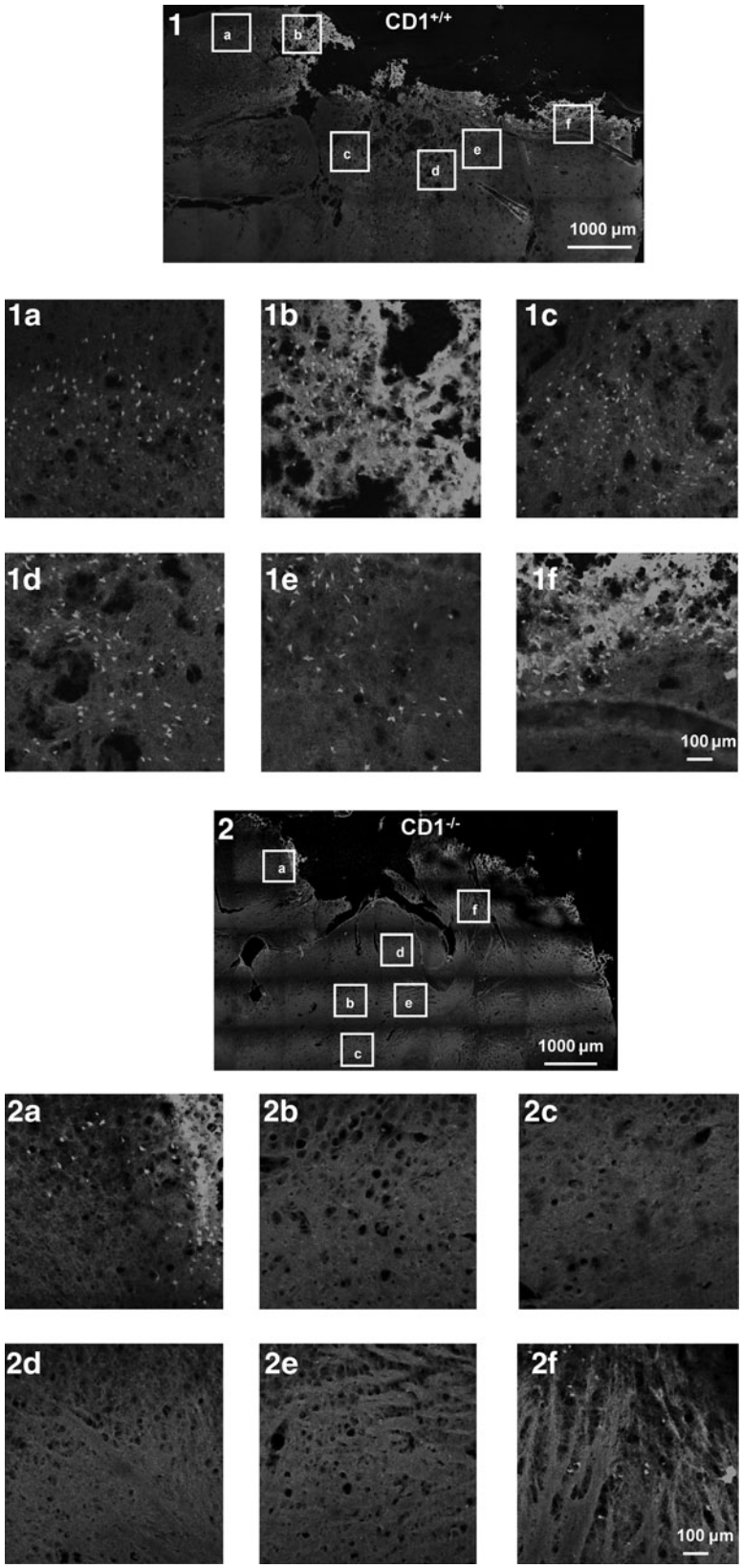

FIG. 1. $CD1^{-/-}$ mice have reduced neurodegeneration after traumatic brain injury (TBI). Fluoro-Jade B staining for qualitative assessment of neuronal degeneration at 24 h post-TBI. The representative confocal images from $CD1^{+/+}$ mice demonstrate degenerating neurons (Fluoro-Jade B-positive) around the lesion injury site (**1a**, **b**, and **f**), and in sub-cortical regions (**1c–e**), whereas $CD1^{-/-}$ mice had fewer Fluoro-Jade B-positive neurons at the injury site (**2a** and **f**), and in sub-cortical areas (**2b–e**), indicating attenuated neuronal degeneration. Higher-magnification images from the indicated regions are shown ($n = 3$/group).

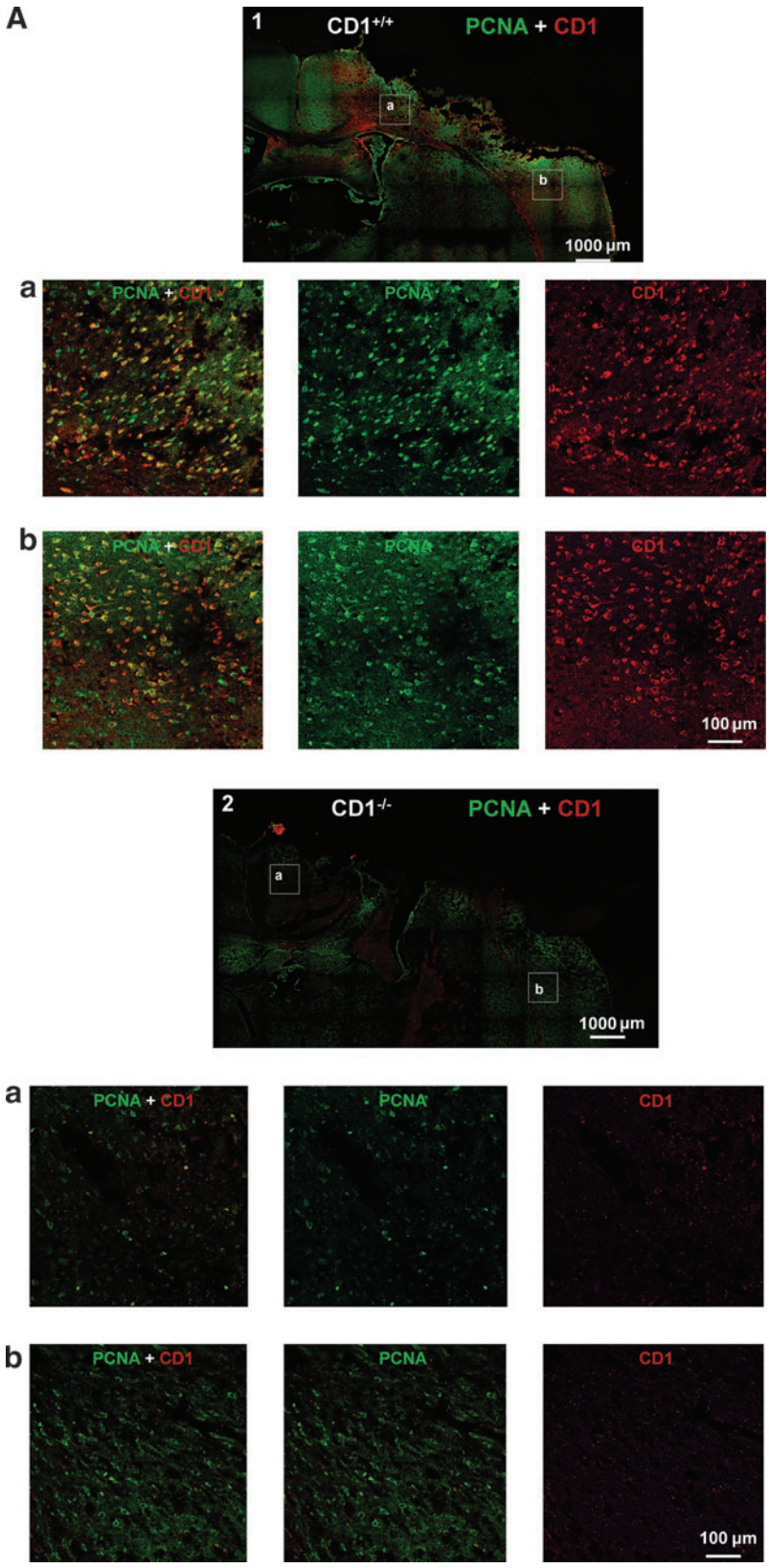

FIG. 2. Traumatic brain injury (TBI)-induced cell cycle activation is diminished in $CD1^{-/-}$ mice. Immunocytochemistry was done for qualitative assessment of cell cycle activation at 24 h after TBI. (**A**) Representative confocal images of the G1 phase cyclin CD1 (red in **1a** and **1b**), and the G1/S phase marker PCNA (green in **1a** and **1b**) showed increased expression of these cell cycle activation markers (yellow) at the lesion site in $CD1^{+/+}$ mice, whereas $CD1^{-/-}$ mice lack CD1 (**2a** and **2b**), and have reduced PCNA (**2a** and **2b**) expression in corresponding regions. (**B**) Representative confocal images of the cell cycle activation marker E2F1 (red in **1a** and **1b**) show increased E2F1 expression at the lesion site in $CD1^{+/+}$ mice, whereas $CD1^{-/-}$ mice had reduced E2F1 (**2a** and **2b**) expression in corresponding regions. 4,6-Diamino-2-phenylindole (DAPI) nuclear staining is shown in blue. Higher-magnification images from the indicated regions are shown ($n = 3$/group). Color image is available online at www.liebertonline.com/neu

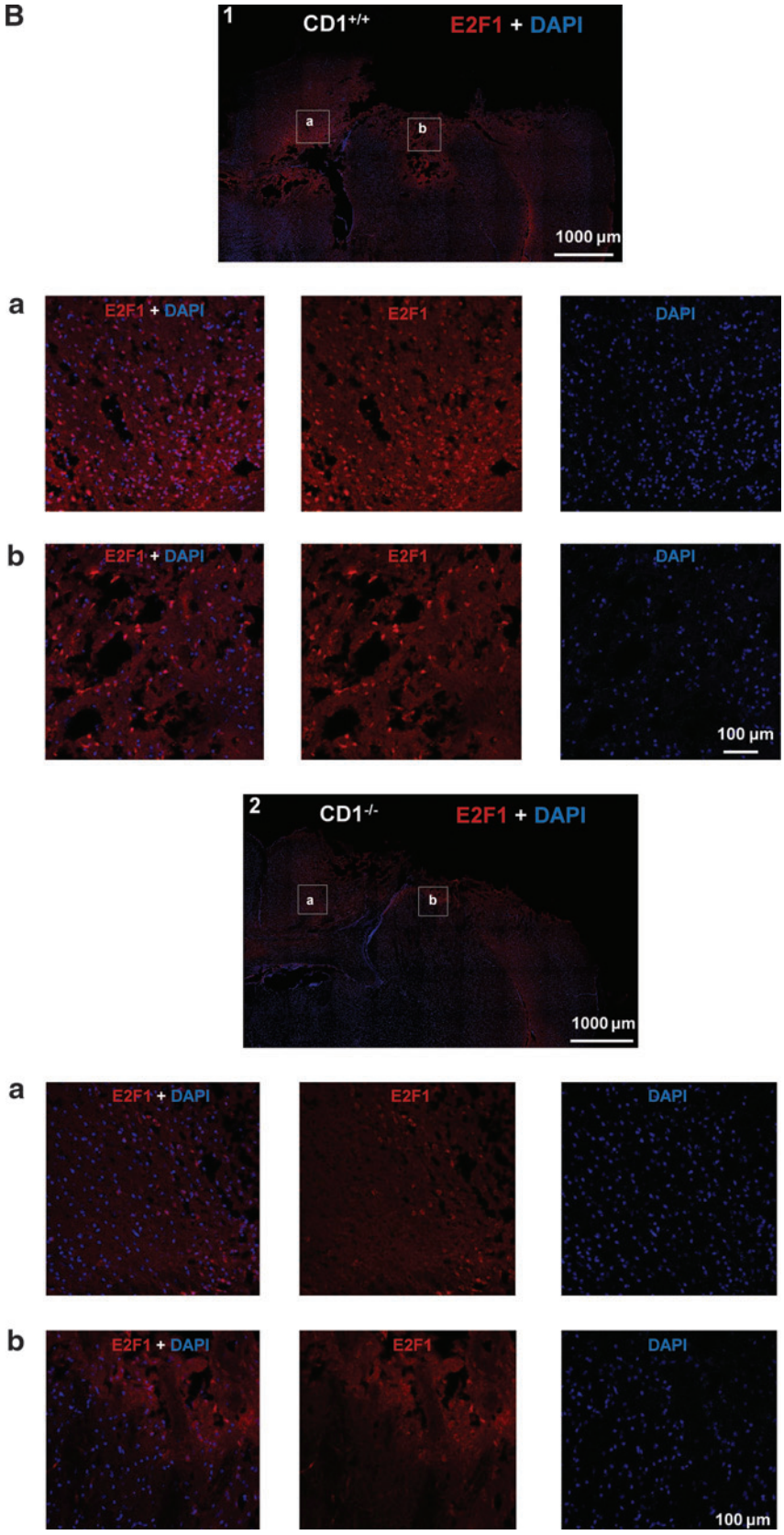

FIG. 2. (*Continued*).

In order to evaluate the role of CCA in the pathophysiology of TBI, we examined three cell cycle markers: CD1, PCNA, and E2F1, at 24 h after injury (Fig. 2A and B). Immunocytochemical analysis revealed increased expression of CD1 (red in Fig. 2A-1, 1a, and 1b), and PCNA (green in Fig. 1, 1a, and 1b), and their co-localization (yellow in Fig. 2A-1 and 2) in the tissue surrounding the lesion site in $CD1^{+/+}$ mice. As expected, $CD1^{-/-}$ mice did not express CD1 (Fig. 2A-1, 2a, and 2b), and had reduced expression of PCNA in the injured hemisphere (Fig. 2A-1, 2a, and 2b). In addition, TBI resulted in increased expression of E2F1 (red in Fig. 2B-1, 1a, and 1b) at the site of the injury in $CD1^{+/+}$mice, which was attenuated in $CD1^{-/-}$ mice in the corresponding areas (Fig. 2B-2, 2a, and 2b) around the lesion.

$CD1^{-/-}$ mice have improved cognitive function after TBI

Spatial learning and memory was tested using the acquisition phase of the MWM test, and the results for latency to find the platform (trial/time) were statistically analyzed by repeated-measures two-way ANOVA (genotype × injury/sham). A significant post-injury day × injury/sham interaction [$F_{(3,112)} = 2.913$, $p = 0.038$] was found. A repeated-measures one-way ANOVA of the data for the acquisition phase of the MWM of the two genotypes in the injured groups indicated that the injured $CD1^{-/-}$ mice showed significantly reduced latency to find the submerged platform compared to the injured $CD1^{+/+}$ mice on post-injury day 17 ($p = 0.028$ versus $CD1^{+/+}$; Fig. 3A), and had a significant improvement in cognitive recovery on post-injury day 17 ($p = 0.007$ versus day 14). There were no statistically significant differences between the sham $CD1^{+/+}$ and $CD1^{-/-}$ groups. Reference memory was assessed using the MWM probe trial on post-injury day 18, and the data for time spent in the target quadrant was statistically analyzed using two-way (genotype × injury/sham) ANOVA. The interaction of genotype × injury/sham was not statistically significant [$F_{(1,26)} = 0.465$, $p = 0.501$]. The factor genotype was also not statistically significant [$F_{(1,26)} = 1.562$, $p = 0.223$]. However, the factor injury/sham was found to be significant [$F_{(1,26)} = 10.389$, $p = 0.003$]. One-tailed paired Student's *t*-test of the data for the two genotypes in the injured groups demonstrated that the injured $CD1^{-/-}$ mice spent more time in the target quadrant compared to the injured $CD1^{+/+}$ mice ($p = 0.0352$ versus $CD1^{+/+}$; Fig. 3B). There were no statistically significant differences between the sham $CD1^{+/+}$ and $CD1^{-/-}$ groups. All TBI-injured mice performed well in the visual cue test, and swim speeds did not differ across groups (data not shown). Retention or intact memory was evaluated using the novel object recognition (NOR) test, and the data for the discrimination index (D.I. %) were statistically analyzed by using two-way ANOVA (genotype × injury/sham). The interaction of

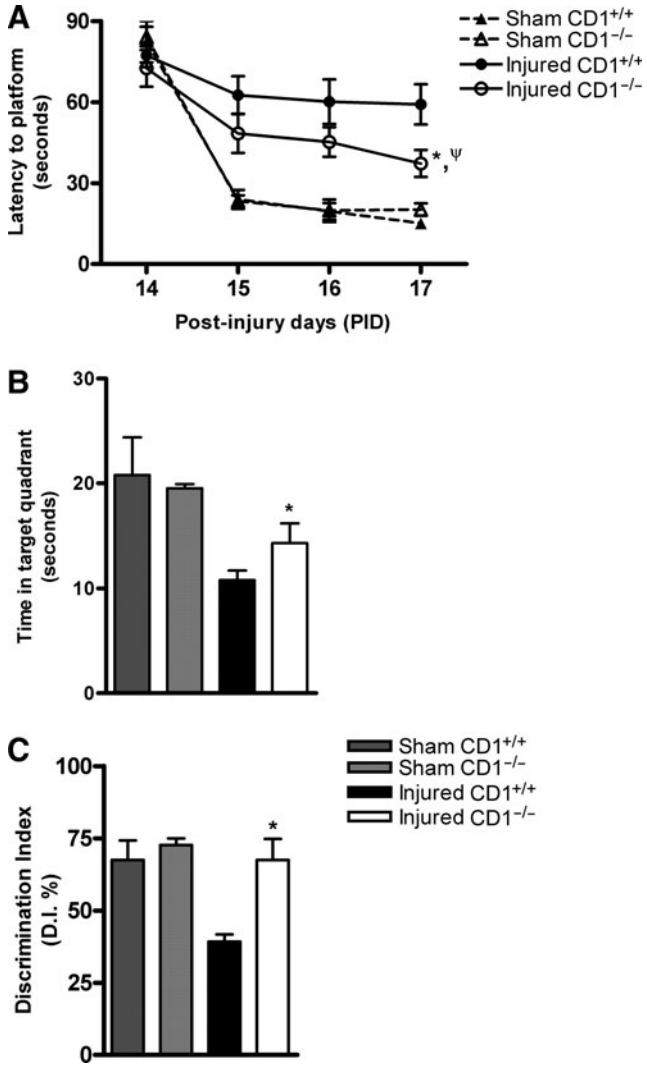

FIG. 3. $CD1^{-/-}$ mice have improved cognitive function following traumatic brain injury (TBI). (**A**) Spatial learning and memory was assessed using the acquisition phase of the Morris Water Maze (MWM) test. $CD1^{-/-}$ mice had reduced (*$p = 0.028$ versus $CD1^{+/+}$ mice) latency to locate the submerged platform on day 17 post-injury, and showed significant improvement ($^{\Psi}p = 0.007$ versus day 14 post-injury) in cognitive recovery. Analysis by repeated-measures two-way analysis of variance (ANOVA), followed by *post-hoc* adjustments using Tukey's test [post-injury day × injury/sham × genotype interaction: $F_{(3,112)} = 0.128$, $p = 0.943$; post-injury day × injury/sham interaction: $F_{(3,112)} = 2.913$, $p = 0.038$]. Repeated-measures one-way ANOVA was done for the sham $CD1^{+/+}$ and $CD1^{-/-}$, and the injured $CD1^{+/+}$ and $CD1^{-/-}$ groups separately, followed by *post-hoc* adjustments using Tukey's test. (**B**) Reference memory was assessed using the probe trial of the MWM test. $CD1^{-/-}$ mice spent more (*$p = 0.0352$ versus $CD1^{+/+}$ mice) time in the target quadrant. Analysis by two-way ANOVA was done, followed by *post-hoc* Tukey's test [genotype × injury/sham interaction: $F_{(1,26)} = 0.465$, $p = 0.501$; injury/sham factor: $F_{(1,26)} = 10.389$, $p = 0.003$; genotype factor: $F_{(1,26)} = 1.562$, $p = 0.223$]. One-tailed paired Student's *t*-test was done for the sham $CD1^{+/+}$ and $CD1^{-/-}$, and the injured $CD1^{+/+}$ and $CD1^{-/-}$ groups separately. (**C**) Retention memory was assessed using novel object recognition (NOR) test. $CD1^{-/-}$ mice showed significantly higher (*$p = 0.0004$ versus $CD1^{+/+}$ mice) discrimination index (D.I. %). Analysis by two-way ANOVA was done, followed by *post-hoc* Tukey's test [genotype × injury/sham interaction: $F_{(1,24)} = 4.569$, $p = 0.043$; injury/sham factor: $F_{(1,24)} = 4.553$, $p = 0.043$]. One-tailed paired Student's *t*-test was done for the sham $CD1^{+/+}$ and $CD1^{-/-}$, and the injured $CD1^{+/+}$ and $CD1^{-/-}$ groups separately (mean ± standard error of the mean; $n = 12$–16/group).

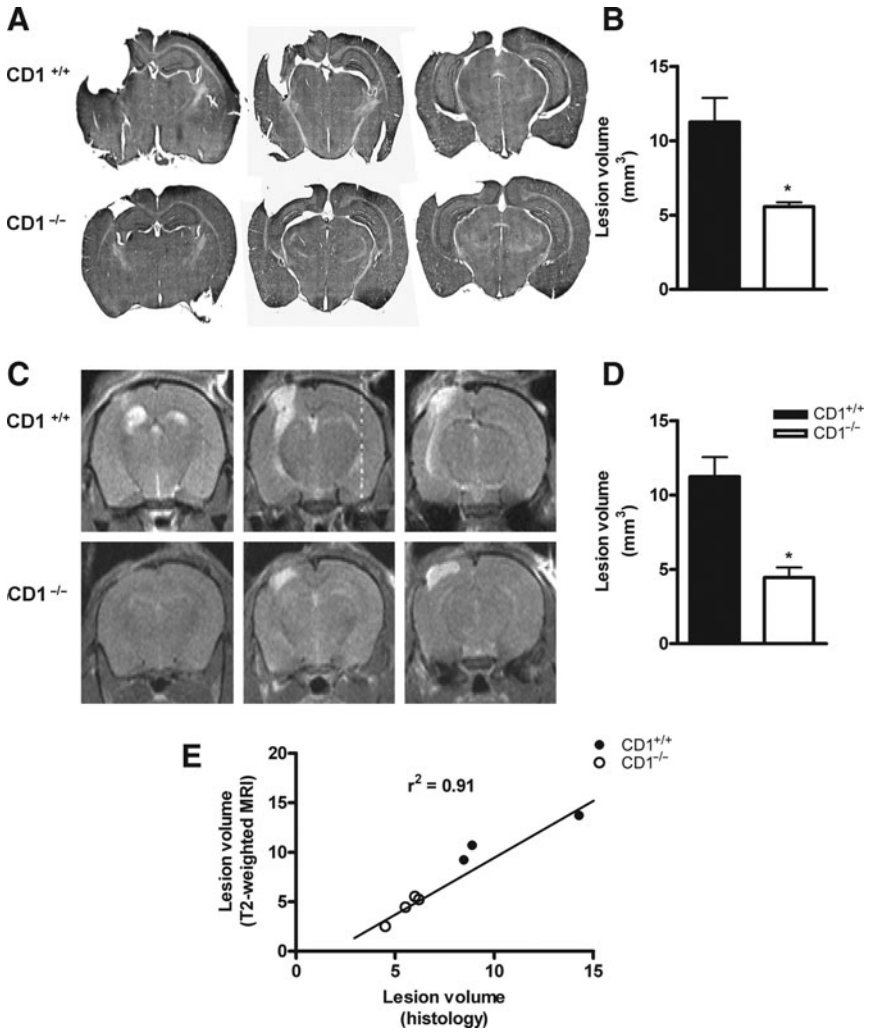

FIG. 4. $CD1^{-/-}$ mice have reduced lesion size following traumatic brain injury (TBI). (**A**) Unbiased stereological assessment of lesion volume at 21 days post-TBI was performed on cresyl violet-stained brain sections. The stained brain sections from $CD1^{-/-}$ animals revealed sparing of hippocampal tissues. (**B**) Lesion quantification. $CD1^{-/-}$ mice had reduced (*$p = 0.004$ versus $CD1^{+/+}$ mice) lesion size at 21 days. Analysis by one-tailed paired Student's *t*-test was done (mean ± standard error of the mean (SEM); $n = 5$–6/group). (**C**) T2-weighted magnetic resonance imaging (MRI) analysis was performed on a subset of animals at 21 days. (**D**) Lesion quantification. $CD1^{-/-}$ mice had decreased (*$p = 0.003$ versus $CD1^{+/+}$ mice) lesion size at 21 days. Analysis by one-tailed paired Student's *t*-test (mean ± SEM; $n = 3$–4/group). (**E**) Linear regression analysis comparing TBI-induced lesion size as quantified by histology and MRI analysis at 21 days post-TBI ($p < 0.0001$ by Pearson's correlation; $r^2 = 0.91$).

genotype × injury/sham was found to be statistically significant [$F_{(1,24)} = 4.569$, $p = 0.043$]. The factor of injury/sham was also statistically significant [$F_{(1,24)} = 4.553$, $p = 0.043$]. One-tailed paired Student's *t*-test of the data for the two genotypes in the injured groups demonstrated that the injured $CD1^{-/-}$ mice had a significantly higher D.I. %, compared with injured $CD1^{+/+}$ mice ($p = 0.0004$ versus $CD1^{+/+}$; Fig. 3C). There were no statistically significant differences between sham-operated $CD1^{+/+}$ and $CD1^{-/-}$ mice in terms of retention memory in the NOR task.

$CD1^{-/-}$ mice have reduced lesion size after TBI

TBI-induced lesion volume was quantified by unbiased stereological techniques. Histological assessment of the cresyl violet-stained brain sections showed that $CD1^{+/+}$ mice developed a large lesion following TBI ($11.3 \pm 1.6\,mm^3$; Fig. 4A and B), whereas the lesion size was significantly reduced in $CD1^{-/-}$ mice ($p = 0.004$ versus $CD1^{+/+}$; $5.6 \pm 0.3\,mm^3$). Significant sparing of the hippocampus was observed in $CD^{-/-}$ mice (Fig. 4A). In addition, *in vivo* T2-weighted MRI analysis was performed on a subset of animals to determine the lesion size in living animals. Consistent with the histological analysis, $CD1^{+/+}$ mice had a large lesion, whereas $CD1^{-/-}$ mice had a significantly reduced lesion size ($CD1^{+/+}$: $11.2 \pm 1.3\,mm^3$, $CD1^{-/-}$: $4.4 \pm 0.7\,mm^3$; $p = 0.003$ versus $CD1^{+/+}$; Fig. 4C and D). There was a positive correlation between TBI-induced lesion size in $CD1^{+/+}$ and $CD1^{-/-}$ mice assessed by unbiased stereology and that determined by *in vivo* T2-weighted MRI ($p < 0.0001$, $r^2 = 0.91$; Fig. 4E).

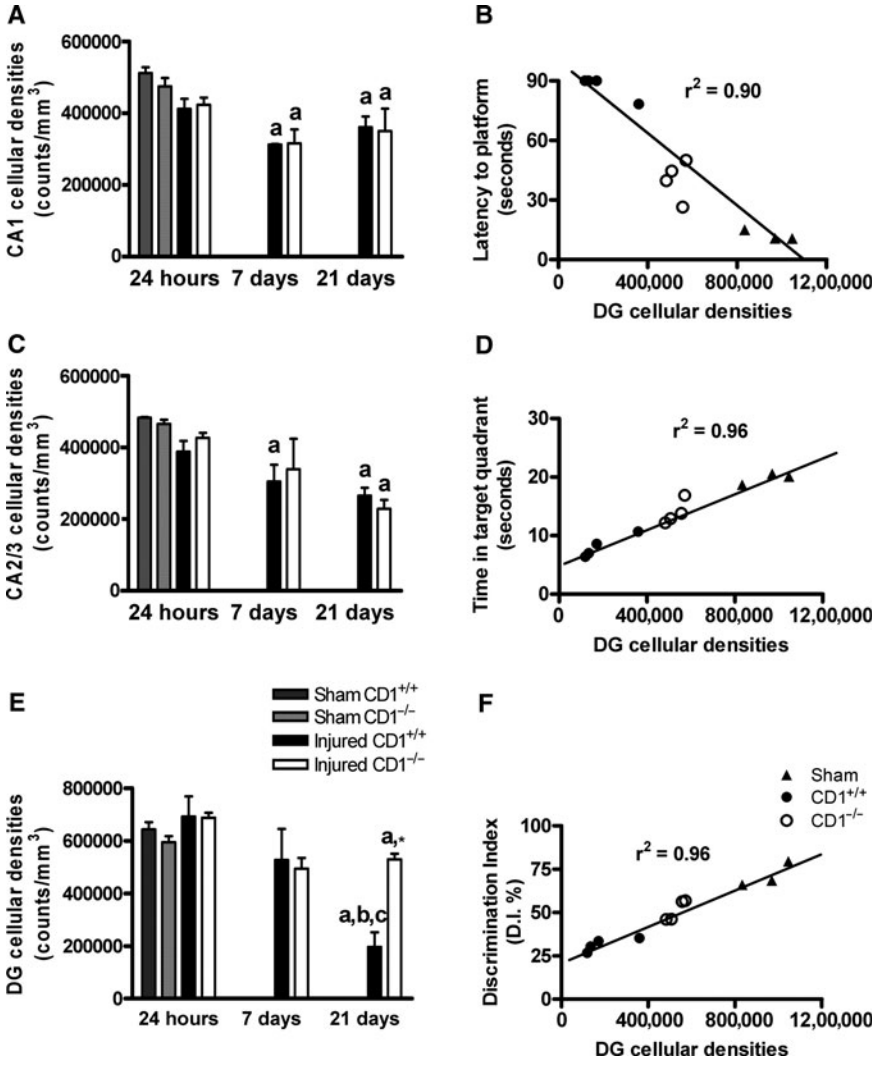

FIG. 5. Progressive neuronal cell loss is attenuated in the dentate gyrus (DG) of $CD1^{-/-}$ mice after traumatic brain injury (TBI). (**A**–**C**) Unbiased stereological quantification of neuronal cell loss in the CA1 (**A**), CA2/3 (**B**), and DG (**C**) sub-regions of the hippocampus at 24 h, 7 days, and 21 days. Neuronal loss was observed in the CA1 and CA2/3 regions within 7 days of the injury, with no significant further loss at 21 days. Progressive neuronal loss was observed in the DG, and $CD1^{-/-}$ mice had attenuated neuronal loss in this region at 21 days ($^{*}p = 0.004$ versus $CD1^{+/+}$ mice). Analysis by one-way analysis of variance (ANOVA) was done with Tukey's *post-hoc* corrections in **A**–**C** for comparisons across different time points. One-tailed paired Student's *t*-test was done for comparison to the $CD1^{+/+}$ group at each time point ($^{a}p < 0.01$ versus sham animals; $^{b}p < 0.001$ versus the 24-h groups; $^{c}p < 0.01$ versus the 7-day groups; mean ± standard error of the mean; $n = 3$–4/group). (**D**) Linear regression analysis comparing TBI-induced neuronal loss in the DG with latency to reach the submerged platform on day 17 post-injury of the Morris Water Maze (MWM). Pearson's correlation ($p < 0.0001$; $r^2 = 0.90$). (**E**) Linear regression analysis comparing TBI-induced neuronal loss in the DG with time spent in the target quadrant in the probe trial of the MWM ($p < 0.0001$ by Pearson's correlation; $r^2 = 0.96$). (**F**) Linear regression analysis was done comparing TBI-induced neuronal loss in the DG with the discrimination index (D.I. %) in the novel object recognition test ($p < 0.0001$ by Pearson's correlation; $r^2 = 0.96$).

$CD1^{-/-}$ mice have reduced neuronal loss in the DG after TBI

Unbiased stereological assessment of surviving neurons in the CA1, CA2/3, and DG sub-regions of the hippocampus at 24 h, and 7 and 21 days after TBI was performed. TBI resulted in significant neuronal loss in the CA1 sub-region of the hippocampus within 7 days post-injury ($p < 0.01$ versus sham animals; Fig. 5A), but additional neuronal loss was not apparent at 21 days. A similar pattern of neuronal loss was observed in the CA2/3 region following TBI, with a non-significant trend toward progressive neuronal loss over time ($p < 0.01$ versus sham animals; Fig. 5B). CD1 knockout failed to protect CA1 or CA2/3 neurons at any time point. In contrast, TBI resulted in significant neuronal losses in the DG of $CD1^{-/-}$ mice at 21 days after TBI ($p < 0.001$ versus sham animals; Fig. 5C). Furthermore, CD1 knockout resulted in significantly improved neuronal survival in the DG at 21 days

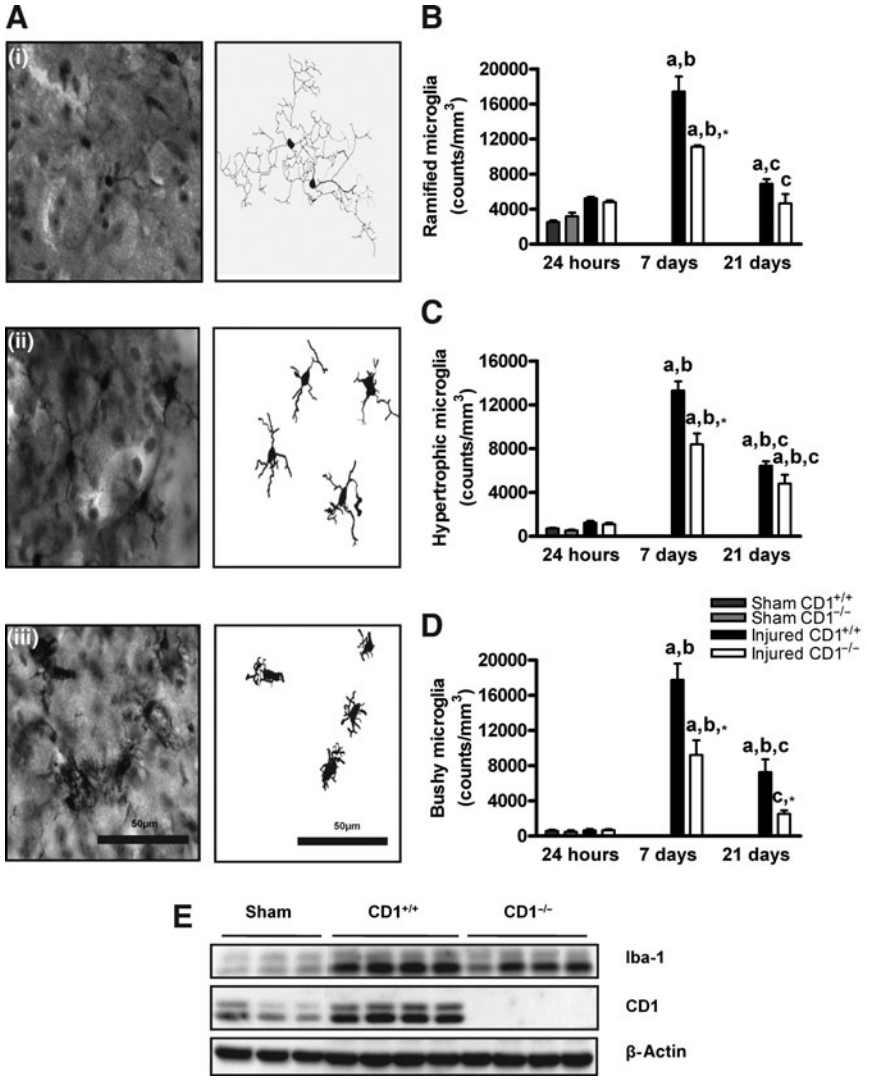

FIG. 6. $CD1^{-/-}$ mice exhibit reduced microglial activation in the cortex after traumatic brain injury (TBI). (**A**) Representative immunohistochemical images and Neurolucida reconstructions of ramified (**i**), hypertrophic (**ii**), and bushy (**iii**) microglia illustrate the different morphological features of each microglial phenotype. (**B**–**D**) Unbiased stereological quantification of microglial cell numbers and activation status in the cortex at 24 h, 7 days, and 21 days post-injury. Ramified (**B**), hypertrophic (**C**), and bushy (**D**) microglial activation phenotypes were analyzed. $CD1^{-/-}$ mice showed reduced ramified ($^*p = 0.03$ versus $CD1^{+/+}$ mice) and hypertrophic microglia ($^*p = 0.02$ versus $CD1^{+/+}$ mice) at 7 days, and attenuated bushy microglia at 7 days ($^*p = 0.008$ versus $CD1^{+/+}$ mice) and 21 days ($^*p = 0.03$ versus $CD1^{+/+}$ mice). Analysis by one-way analysis of variance (ANOVA) was done, followed by *post-hoc* Tukey's test. One-tailed paired Student's *t*-test was done for comparison with the $CD1^{+/+}$ group at each time point ($^a p < 0.01$ versus sham animals; $^b p < 0.05$ versus the 24-h groups; $^c p < 0.05$ versus the 7-day groups; mean ± standard error of the mean; $n = 3$–4/group). (**E**) Western blot analysis of cortical tissues for the microglial activation marker Iba-1 and CD1. $CD1^{-/-}$ mice had significantly reduced Iba-1 expression at 21 days after TBI. CD1 expression was significantly increased at 21 days post-TBI, and was absent in $CD1^{-/-}$ mice.

($p = 0.004$ versus $CD1^{+/+}$) after injury compared with the $CD1^{+/+}$ group (529,749 ± 20,732 versus 196,138 ± 55,558 counts/mm^3 for the $CD1^{-/-}$ and $CD1^{+/+}$ groups, respectively; Fig. 5C). There were no significant differences in CA1, CA2/3, and DG neuronal cellular densities between sham-injured $CD1^{+/+}$ and $CD1^{-/-}$ mice (Fig. 5A, B, and C). In addition, there was a strong correlation ($p < 0.0001$) between improved cognitive performance in the MWM acquisition phase ($r^2 = 0.90$; Fig. 5D), probe trial ($r^2 = 0.96$; Fig. 5E), and NOR test ($r^2 = 0.96$; Fig. 5F), and reduced neuronal cell loss in the DG due to CD1 knockout.

$CD1^{-/-}$ mice have reduced microglial activation in the injured cortex following TBI

Brain injury results in a switch in microglial phenotype, from a resting form displaying ramified cellular morphologies, to more activated forms displaying hypertrophic or bushy morphologies, with the latter being the most reactive (Davis et al., 1994; Soltys et al., 2001; Zhan et al., 2008; Fig. 6). Stereological assessment of microglial cell number and activation phenotype was performed in the cortex at 24 h, 7 days, and 21 days after TBI. There was a significant increase in

ramified microglia in both injured groups at 7 days post-TBI compared to sham controls, which remained elevated in the $CD1^{+/+}$ group through 21 days ($p<0.01$ versus sham animals; Fig. 6B). TBI resulted in a significant and sustained increase in hypertrophic microglia at 7 and 21 days post-injury ($p<0.001$ versus sham animals; Fig. 6C). There was a marked increase in bushy microglia observed at 7 days post-injury, which was sustained through 21 days in the $CD1^{+/+}$ group ($p<0.001$ versus sham; Fig. 6D). CD1 knockout significantly reduced ramified ($p=0.03$ versus $CD1^{+/+}$; 11,128 ± 146 versus 17,419 ± 1719 counts/mm^3), and hypertrophic ($p=0.02$ versus $CD1^{+/+}$; 8384 ± 1003 versus 13,293 ± 841 counts/mm^3) microglia at 7 days post-TBI compared to $CD1^{+/+}$ samples (Fig. 6B and C). In addition, the $CD1^{-/-}$ group had significant attenuation of bushy microglia at 7 days ($p=0.008$ versus $CD1^{+/+}$; 9221 ± 1665 versus 17,764 ± 1841 counts/mm^3), and 21 days ($p=0.03$ versus $CD1^{+/+}$; 2522 ± 407 versus 7257 ± 1468 counts/mm^3), compared to $CD1^{+/+}$ mice after injury (Fig. 6D). There were no significant differences in ramified, hypertrophic, and bushy microglial densities between sham-injured $CD1^{+/+}$ and $CD1^{-/-}$ mice (Fig. 6B, C, and D).

In addition, Western immunoblotting for the activated microglial marker Iba-1 was performed in the cortical extracts from $CD1^{+/+}$ and $CD1^{-/-}$ mice at 21 days after TBI. As expected, TBI increased the expression of Iba-1 in cortical extracts from $CD1^{+/+}$mice ($p<0.001$ versus sham animals; 3.1 ± 0.09 versus 1 ± 0.1 arbitrary units), whereas the TBI-induced increase in Iba-1 was significantly reduced in $CD1^{-/-}$ cortical extracts ($p=0.014$ versus $CD1^{+/+}$; Fig. 6E). Western immunoblotting for CD1 confirmed the lack of CD1 expression in $CD^{-/-}$ mice, and demonstrated that CD1 expression remained significantly induced in $CD1^{+/+}$ mice at 21 days after injury ($p=0.047$ versus sham; 2.4 ± 0.2 versus 1.2 ± 0.3 arbitrary units).

Discussion

Our data confirm the important role of cell cycle activation (CCA) in secondary injury after TBI, and show that knocking out the cyclin D1 (CD1) gene limits cell-cycle progression and reduces the extent of trauma-induced neurological damage and related functional deficits. The use of quantitative stereological assessment to address regional neuronal loss over time and its temporal/anatomic associations with both cognitive performance and microglial phenotype are also noteworthy.

A role for CCA in the pathophysiology of CNS trauma has been suggested previously (Byrnes and Faden, 2007; Byrnes et al., 2007; Cernak et al., 2005; Giovanni et al., 2005; Hilton et al., 2008), but here we more specifically address the role of CD1 in this process. The members of the cyclin D family (D1, D2, and D3) bind and allosterically regulate CDK4 and CDK6 (Sherr and Roberts, 2004). In addition, D-type cyclins modulate cyclin E and indirectly affect CDK2 activity (Sherr and Roberts, 2004), by titration of the endogenous CDK inhibitors $p27^{Cip1}$ and $p27^{Kip1}$ from cyclin E/CDK2 complexes (Cheng et al., 1998; Reynisdottir et al., 1995; Swanton, 2004). In particular, CD1, a G1-phase multifunctional cyclin, accumulates in the nuclei of dividing cells and translocates as the cells enter the S-phase (Baldin et al., 1993). Microinjection of antibodies or anti-sense plasmids against CD1 has been shown to cause cell cycle inhibition by preventing the cells from entering S-phase (Baldin et al., 1993). Previous studies have linked CD1 with neuronal death and neurodegeneration in models of cerebral ischemia (Li et al., 1997; Small et al., 2001; Zhu et al., 2007), spinal cord injury (Byrnes and Faden, 2007), and Alzheimer's disease (Raina et al., 2000).

Pharmacological inhibitors of CDKs have been used to elucidate the role of cell-cycle mechanisms (Cernak et al., 2005; Giovanni et al., 2005; Hilton et al., 2008). A critical limitation of this approach is that most of these compounds inhibit the activity of multiple CDKs and often other classes of protein kinases (Bain et al., 2007). In contrast, genetic approaches such as those used in this study can selectively and specifically target a single cell-cycle molecule in order to determine its effects. Genetic ablation of CD1 has been found to have neuroprotective effects in experimental stroke and spinal cord injury (Byrnes and Faden, 2007; Rashidian et al., 2005; Zhu et al., 2007). Cerebellar granule neurons from $CD1^{-/-}$ mice have been shown to exhibit a higher degree of resistance to hypoxic insult in an *in vitro* model of neuronal cell death in the presence of NMDA antagonist MK801 than their littermate controls (Rashidian et al., 2005). Knocking out the CD1 gene has been found to inhibit astrocyte proliferation and neuronal apoptosis, and to reduce lesion size in a model of focal cerebral ischemia (Zhu et al., 2007). Similarly, a preliminary study of $CD1^{-/-}$ mice in a model of spinal cord injury showed less hindlimb paralysis and reduced lesion volume at 72 h post-injury (Byrnes and Faden, 2007).

We have previously reported elevated levels of CD1 in the cortex within 24 h after fluid percussion-induced TBI in rats, which was associated with neuronal cell death (Giovanni et al., 2005). Here we demonstrate increased expression of CD1 at 24 h after injury in $CD1^{+/+}$ mice, co-localizing with elevated PCNA expression. PCNA is a marker of late G1/early S-phase during cell cycle progression (Byrnes and Faden, 2007; Stoica et al., 2009), and its role in neuronal death has been suggested in models of neurodegeneration and excitotoxicity (Verdaguer et al., 2004; Yang et al., 2001). Increased expression of these cell-cycle markers after TBI appears to occur within the neurons, as indicated by the morphology of neurons on the representative confocal images. We also observed elevated expression of E2F1 transcription factor at 24 h after TBI in $CD1^{+/+}$ mice. E2F transcription factors induce apoptosis in neurons via activation of B- and C-myb genes (Liu et al., 2004), and induce expression of caspases-3, −9, and −8, and Apaf-1 (Nahle et al., 2002), as well asp53 and p73 activation (Greene et al., 2004). In addition, we demonstrate that CD1 expression remains elevated at least until 21 days post-injury. $CD1^{-/-}$ mice do not express CD1, and CCA after TBI in these animals is attenuated, as indicated by reduced expression of PCNA and E2F1 at 24 h after TBI.

To assess neuronal survival after TBI, we performed Fluoro-Jade B staining at 24 h. $CD1^{+/+}$ mice showed extensive neurodegeneration, as indicated by dense Fluoro-Jade B-positive neurons not only around the lesion site, but also within the sub-cortical regions. Our observation is in agreement with previous studies that have suggested that ischemia- and CCI-induced damage to the cortex may cause retrograde degeneration of neurons in sub-cortical regions, such as the thalamus (Hall et al., 2005; Iizuka et al., 1990). Importantly, the general areas in the injured hemisphere with increased Fluoro-Jade B staining often coincided with regions exhibiting increased expression of the cell cycle markers CD1,

PCNA, and E2F1. In contrast, $CD1^{-/-}$ mice demonstrated fewer degenerating neurons as well as less intense markers of CCA.

In order to better understand TBI-induced neurodegeneration, we quantified neuronal cellular densities (number of neurons per unit volume) as a measure of neuronal loss in the CA1, CA2/3, and DG sub-regions of the hippocampus using unbiased stereological techniques. This is to our knowledge the first detailed and unbiased analysis of progressive neuronal loss in specific regions of the hippocampus following mouse CCI. Considerable neuronal loss in the CA1 and CA2/3 regions occurred by 7 days post-injury, followed by an insignificant further loss at 21 days, suggesting the limited duration of secondary injury in these regions. In contrast, neuronal loss in the DG was more modest through the first 7 days after injury, but was followed by a significant neuronal loss at 21 days, indicating progressive secondary injury processes in this region. $CD1^{-/-}$ mice showed significantly less neuronal loss at 21 days in the DG region than wild-type controls, but no differences in the CA1 and CA2/3 regions. CD1 knockout significantly attenuated cognitive deficits in the acquisition trials and probe test of the MWM tasks of spatial learning and reference memory, respectively. Improved cognitive performance in the MWM serves as a potential indicator of reduced hippocampal damage (Redish and Touretzky, 1998). $CD1^{-/-}$ mice also showed a significant improvement in cognitive performance in the NOR test of retention memory. Improvements in cognitive outcomes in the NOR test indicate reduced hippocampal damage (Akirav and Maroun, 2006; Broadbent et al., 2010). The relative contribution and significance of different hippocampal subregions in encoding and retrieval of learning and memory function can be quantified by counting neuronal cells in these regions (Gilbert and Brushfield, 2009; Lee and Kesner, 2004). Our data show a strong positive correlation between improvement in cognitive function using different behavioral tests and increased neuronal survival in the DG region of the hippocampus in the $CD1^{-/-}$ group (Fig 5D-F). The close correlation between improved cognition and reduced DG neuronal cell loss underscores the importance of the DG subregion of the hippocampus in the formation of spatial learning, reference, and retention memory (Lee and Kesner, 2004; Lee et al., 2005), and indicates that trauma-induced loss of neurons in this region contributes to cognitive impairment. Critically, the region (DG) showing the most persistent secondary injury is also the most susceptible to the CD1-targeted intervention.

The size of the cortical lesion provides a marker for secondary injury-mediated tissue damage and neurodegeneration. Unbiased stereology and T2-weighted MRI analysis were used to quantify the lesion volume after TBI, and the data obtained from both methods showed a significant reduction in lesion size in $CD1^{-/-}$ mice, compared with the $CD1^{+/+}$ group. Regression analysis demonstrated a strong correlation between reduced estimates of lesion volume evaluated by MRI and stereological techniques, indicating the highly comparable potential of both these techniques in lesion size estimation.

Chronic inflammation following CNS trauma may provide a mechanistic link between early and chronic neurodegeneration (Nandoe, 2002). In order to better assess the neuroinflammatory response after brain trauma we performed a quantitative assessment of microglial activation following TBI. Microglial activation status was based on morphological features using unbiased stereology, and we determined microglial cell density (the number of cells of each phenotype per unit of volume) in the injured cortex at various time points following injury. Although both neuroprotective and neurotoxic microglial phenotypes have been described (Davis et al., 1994; Loane and Byrnes, 2010; Soltys et al., 2001), microglial activation and the release of associated inflammatory factors has been proposed as an important contributing factor in chronic neurodegenerative disorders, including Alzheimer's disease (Eikelenboom et al., 2002). Our previous studies have indicated that sustained microglial activation after CNS trauma may play a role in neuronal cell loss following the release of neurotoxic molecules such as NO (Byrnes and Faden, 2007; Byrnes et al., 2007). Based on morphology, microglia can be classified into three categories corresponding to increasing activation status: ramified (resting), hypertrophic, and bushy (Davis et al., 1994; Soltys et al., 2001; Zhan et al., 2008). Ramified microglia (Fig. 6A) have small cell bodies with thin and highly branched processes. In contrast, hypertrophic microglia (Fig. 6A) have larger cell bodies with thicker and shorter processes (Zhan et al., 2008), whereas bushy microglia (Fig. 6A) have multiple short processes that form thick bundles around enlarged cell bodies (Zhan et al., 2008). CNS injury causes transformation of ramified microglia into more active phenotypes, such as hypertrophic and bushy forms (Soltys et al., 2001). The relative proportion of each microglial phenotype determines the extent of microglial activation and inflammation. This is to our knowledge the first detailed analysis of progressive microglial activation in the cortex following CCI. In this study, we observed significant increases in ramified as well as activated hypertrophic and bushy microglial phenotypes at 7 days following brain trauma. No significant changes were detected at 24 h post-injury in any phenotype, suggesting that this process is relatively delayed. The numbers of all microglial types were decreased 21 days after injury compared to earlier time points, but remained significantly elevated compared to sham controls at this time point, underscoring the chronic nature of such microglial activation. We demonstrated that cell-cycle inhibition via genetic ablation of CD1 significantly attenuated microglial activation, as indicated by the reduced numbers of ramified and hypertrophic microglia seen at 7 days, and bushy microglia at both 7 and 21 days after TBI. In addition, our data demonstrate elevated protein levels of the reactive microglial marker Iba-1 in both injured groups at 21 days after injury. $CD1^{-/-}$ mice showed a significant reduction in Iba-1 expression compared to wild-type controls, underscoring a role of CD1 in microglial activation.

In conclusion, our findings demonstrate the progressive nature of neurodegeneration and neuroinflammation following TBI. Genetic ablation of the CD1 gene reduced progressive neuronal cell loss/neurodegeneration in the hippocampus, and attenuated microglial activation/neuroinflammation in the cortex. $CD1^{-/-}$ mice also exhibited improved cognitive recovery, reduced lesion size, and attenuated neuronal cell death and expression of markers of CCA following TBI. The effects of genetically knocking out the CD1 gene and inhibiting cell-cycle pathways likely reflect its multipotential neuroprotective activities due to direct inhibitory effects on CCA-dependent neuronal cell death, as well as microglial-mediated

neuroinflammation. Thus our study provides further evidence that cell-cycle inhibition, via potentially targeting CD1, may be a promising therapeutic strategy for the treatment of TBI.

Acknowledgments

We thank Kelly Wilson, Nicole Hockenbury, Michael Dinizo, David Knipp, and Michael Murray for expert technical assistance. This work was supported by a grant from the National Institutes of Health (R01 NS052568).

Author Disclosure Statement

No competing financial interests exist.

References

Akirav, I., and Maroun, M. (2006). Ventromedial prefrontal cortex is obligatory for consolidation and reconsolidation of object recognition memory. Cereb. Cortex 16, 1759–1765.

Arendt, T. (2003). Synaptic plasticity and cell cycle activation in neurons are alternative effector pathways: the 'Dr. Jekyll and Mr. Hyde concept' of Alzheimer's disease or the yin and yang of neuroplasticity. Prog. Neurobiol. 71, 83–248.

Bain, J., Plater, L., Elliott, M., Shapiro, N., Hastie, C., McLauchlan, H., Klevernic, I., Arthur, J., Alessi, D. and Cohen, P. (2007). The selectivity of protein kinase inhibitors: a further update. Biochem. J. 408, 297–315.

Baldin, V., Lukas, J., Marcote, M., Pagano, M. and Draetta, G. (1993). Cyclin D1 is a nuclear protein required for cell cycle progression in G1. Genes Dev. 7, 812–821.

Bevins, R., and Besheer, J. (2006). Object recognition in rats and mice: a one-trial non-matching-to-sample learning task to study 'recognition memory'. Nat. Protoc. 1, 1306–1311.

Bramlett, H., and Dietrich, W. (2007). Progressive damage after brain and spinal cord injury: pathomechanisms and treatment strategies. Prog. Brain Res. 161, 125–141.

Broadbent, N.J., Gaskin, S., Squire, L.R. and Clark, R.E. (2010). Object recognition memory and the rodent hippocampus. Learn. Mem. 17, 5–11.

Byrnes, K., and Faden, A. (2007). Role of cell cycle proteins in CNS injury. Neurochem. Res. 32, 1799–1807.

Byrnes, K., Stoica, B., Fricke, S., Di Giovanni, S., and Faden, A. (2007). Cell cycle activation contributes to post-mitotic cell death and secondary damage after spinal cord injury. Brain 130, 2977–2992.

Cernak, I., Stoica, B., Byrnes, K., Di Giovanni, S., and Faden, A. (2005). Role of the cell cycle in the pathophysiology of central nervous system trauma. Cell Cycle 4, 1286–1293.

Cheng, M., Sexl, V., Sherr, C.J., and Roussel, M.F. (1998). Assembly of cyclin D-dependent kinase and titration of p27Kip1 regulated by mitogen-activated protein kinase kinase (MEK1). Proc. Natl. Acad. Sci. USA 95, 1091–1096.

Davis, E., Foster, T., and Thomas, W. (1994). Cellular forms and functions of brain microglia. Brain Res. Bull. 34, 73–78.

Dutton, R., Stansbury, L., Leone, S., Kramer, E., Hess, J., and Scalea, T. (2010). Trauma mortality in mature trauma systems: are we doing better? An analysis trauma mortality patterns, 1997–2008. J. Trauma 69, 620–626.

Eikelenboom, P., Bate, C., Van Gool, W., Hoozemans, J., Rozemuller, J., Veerhuis, R., and Williams, A. (2002). Neuroinflammation in Alzheimer's disease and prion disease. Glia 40, 232–239.

Faden, A., Knoblach, S., Cernak, I., Fan, L., Vink, R., Araldi, G., Fricke, S., Roth, B., and Kozikowski, A. (2003). Novel diketopiperazine enhances motor and cognitive recovery after traumatic brain injury in rats and shows neuroprotection in vitro and in vivo. J. Cereb. Blood Flow Metab. 23, 342–354.

Fantl, V., Stamp, G., Andrews, A., Rosewell, I., and Dickson, C. (1995). Mice lacking cyclin D1 are small and show defects in eye and mammary gland development. Genes Dev. 9, 2364–2372.

Faul, M., Xu, L., Wald, M., and Coronado, V. (2010). Traumatic brain injury in the United States: Emergency department visits, hospitalizations and deaths 2002–2006. Atlanta, GA: Centers for Disease Control and Prevention National Center for Injury Prevention and Control.

Fox, G.B., Fan, L., Levasseur, R.A., and Faden, A.I. (1998). Sustained sensory/motor and cognitive deficits with neuronal apoptosis following controlled cortical impact brain injury in the mouse. J. Neurotrauma 15, 599–614.

Freeman, R.S., Estus, S., and Johnson, E.M., Jr. (1994). Analysis of cell cycle-related gene expression in postmitotic neurons: selective induction of cyclin D1 during programmed cell death. Neuron 12, 343–355.

Gilbert, P.E., and Brushfield, A.M. (2009). The role of the CA3 hippocampal subregion in spatial memory: a process oriented behavioral assessment. Prog. Neuropsychopharmacol. Biol. Psychiatry 33, 774–781.

Giovanni, S.D., Movsesyan, V., Ahmed, F., Cernak, I., Schinelli, S., Stoica, B., and Faden, A. (2005). Cell cycle inhibition provides neuroprotection and reduces glial proliferation and scar formation after traumatic brain injury. Proc. Natl. Acad. Sci. USA 102, 8333–8338.

Greene, L., Biswas, S., and Liu, D. (2004). Cell cycle molecules and vertebrate neuron death: E2F at the hub. Cell Death Differ. 11, 49–60.

Hall, E.D., Sullivan, P.G., Gibson, T.R., Pavel, K.M., Thompson, B.M., and Scheff, S.W. (2005). Spatial and temporal characteristics of neurodegeneration after controlled cortical impact in mice: more than a focal brain injury. J. Neurotrauma 22, 252–265.

Herrup, K., and Yang, Y. (2007). Cell cycle regulation in the postmitotic neuron: oxymoron or new biology? Nat. Rev. Neurosci. 8, 368–378.

Hilton, G.D., Stoica, B.A., Byrnes, K.R., and Faden, A.I. (2008). Roscovitine reduces neuronal loss, glial activation, and neurologic deficits after brain trauma. J. Cereb. Blood Flow Metab. 28, 1845–1859.

Iizuka, H., Sakatani, K., and Young, W. (1990). Neural damage in the rat thalamus after cortical infarcts. Stroke 21, 790–794.

Kranenburg, O., vanderEb, A., and Zantema, A. (1996). Cyclin D1 is an essential mediator of apoptotic neuronal cell death. EMBO J. 15, 46–54.

Landis, M.W., Pawlyk, B.S., Li, T., Sicinski, P., and Hinds, P.W. (2006). Cyclin D1-dependent kinase activity in murine development and mammary tumorigenesis. Cancer Cell 9, 13–22.

Lee, I., and Kesner, R. (2004). Encoding versus retrieval of spatial memory: double dissociation between the dentate gyrus and the perforant path inputs into CA3 in the dorsal hippocampus. Hippocampus 14, 66–76.

Lee, I., Hunsaker, M.R., and Kesner, R.P. (2005). The role of hippocampal subregions in detecting spatial novelty. Behav. Neurosci. 119, 145–153.

Liu, D.X., Biswas, S.C., and Greene, L.A. (2004). B-myb and C-myb play required roles in neuronal apoptosis evoked by nerve growth factor deprivation and DNA damage. J. Neurosci. 24, 8720–8725.

Li, Y., Chopp, M., Powers, C., and Jiang, N. (1997). Immunoreactivity of cyclin D1/cdk4 in neurons and oligodendrocytes after focal cerebral ischemia in rat. J. Cereb. Blood Flow Metab. 17, 846–856.

Loane, D.J., and Byrnes, K.R. (2010). Role of microglia in neurotrauma. Neurotherapeutics 7, 366–377.

Loane, D.J., and Faden, A.I. (2010). Neuroprotection for traumatic brain injury: translational challenges and emerging therapeutic strategies. Trends Pharmacol. Sci. 31, 596–604.

Loane, D.J., Pocivavsek, A., Moussa, C.E., Thompson, R., Matsuoka, Y., Faden, A.I., Rebeck, G.W., and Burns, M.P. (2009). Amyloid precursor protein secretases as therapeutic targets for traumatic brain injury. Nat. Med. 15, 377–379.

Nahle, Z., Polakoff, J., Davuluri, R.V., McCurrach, M.E., Jacobson, M.D., Narita, M., Zhang, M.Q., Lazebnik, Y., Bar-Sagi, D., and Lowe, S.W. (2002). Direct coupling of the cell cycle and cell death machinery by E2F. Nat. Cell Biol. 4, 859–864.

Nandoe, R. (2002). Head trauma and Alzheimer's disease. J. Alzheimer's Dis. 4, 303–308.

Nguyen, M., Boudreau, M., Kriz, J., Couillard-Despres, S., Kaplan, D., and Julien, J. (2003). Cell cycle regulators in the neuron death pathway of amyotrophic lateral sclerosis caused by mutant superoxide dismutase. J. Neurosci. 23, 2131–2140.

Raina, A.K., Zhu, X., Rottkamp, C.A., Monteiro, M., Takeda, A., and Smith, M.A. (2000). Cyclin' toward dementia: cell cycle abnormalities and abortive oncogenesis in Alzheimer disease. J. Neurosci. Res. 61, 128–133.

Rashidian, J., Iyirhiaro, G., Aleyasin, H., Rios, M., Vincent, I., Callaghan, S., Bland, R.J., Slack, R.S., During, M.J., and Park, D.S. (2005). Multiple cyclin-dependent kinases signals are critical mediators of ischemia/hypoxic neuronal death in vitro and in vivo. Proc. Natl. Acad. Sci. USA 102, 14080–14085.

Redish, A.D., and Touretzky, D.S. (1998). The role of the hippocampus in solving the Morris water maze. Neural Comput. 10, 73–111.

Reynisdottir, I., Polyak, K., Iavarone, A., and Massague, J. (1995). Kip/Cip and Ink4 Cdk inhibitors cooperate to induce cell cycle arrest in response to TGF-beta. Genes Dev. 9, 1831–1845.

Sherr, C., and Roberts, J. (2004). Living with or without cyclins and cyclin-dependent kinases. Genes Dev. 18, 2699–2711.

Sicinski, P., Donaher, J., Parker, S., Li, T., Fazeli, A., Gardner, H., Haslam, S., Elledge, S., and Weinberg, R. (1995). Cyclin D1 provides a link between development and oncogenesis in the retina and breast. Cell 82, 621–630.

Small, D.L., Monette, R., Fournier, M.C., Zurakowski, B., Fiander, H., and Morley, P. (2001). Characterization of cyclin D1 expression in a rat global model of cerebral ischemia. Brain Res. 900, 26–37.

Soltys, Z., Ziaja, M., Pawlinski, R., Setkowicz, Z., and Janeczko, K. (2001). Morphology of reactive microglia in the injured cerebral cortex. Fractal analysis and complementary quantitative methods. J. Neurosci. Res. 63, 90–97.

Stoica, B.A., Byrnes, K.R., and Faden, A.I. (2009). Cell cycle activation and CNS injury. Neurotox. Res. 16, 221–237.

Swanton, C. (2004). Cell-cycle targeted therapies. Lancet Oncol 5, 27–36.

Verdaguer, E., Jimenez, A., Canudas, A.M., Jorda, E.G., Sureda, F.X., Pallas, M., and Camins, A. (2004). Inhibition of cell cycle pathway by flavopiridol promotes survival of cerebellar granule cells after an excitotoxic treatment. J. Pharmacol. Exp. Ther. 308, 609–616.

Yang, Y., Mufson, E., and Herrup, K. (2001). Neuronal cell death is preceded by cell cycle events at all stages of Alzheimer's disease. J. Neurosci. 23, 2557–2563.

Zhan, X., Kim, C., and Sharp, F. (2008). Very brief focal ischemia simulating transient ischemic attacks (TIAs) can injure brain and induce Hsp70 protein. Brain Res, 1234, 184–197.

Zhu, Z., Zhang, Q., Yu, Z., Zhang, L., Tian, D., Zhu, S., Bu, B., Xie, M., and Wang, W. (2007). Inhibiting cell cycle progression reduces reactive astrogliosis initiated by scratch injury in vitro and by cerebral ischemia in vivo. Glia 55, 546–558.

Address correspondence to:
Alan I. Faden, M.D.
Shock Trauma and Anesthesiology Research (STAR)
Organized Research Center
419 West Redwood Street, Suite 225
Baltimore, MD 21201

E-mail: afaden@anes.umm.edu